Steel and Composite Structures, *Vol. 32, No. 1 (2019) 37-57*
DOI: https://doi.org/10.12989/scs.2019.32.1.037

Lateral performance of CRCS connections with tube plate

Rahman Jafari [1b], Nader K.A. Attari [*2], Ali Nikkhoo [3a] and Saeid Alizadeh [4c]

[1] *Civil Engineering Department, University of Science and Culture, Tehran, Iran*
[2] *Structural Engineering Department, Road, Housing, and Urban Development Research Center, Tehran, Iran*
[3] *Civil Engineering Department, University of Science and Culture, Tehran, Iran*
[4] *Civil Engineering Department, University of Canterbury, Christchurch, New Zealand*

(*Received June 24, 2018, Revised April 8, 2019, Accepted May 22, 2019*)

Abstract. This paper presents experimental and analytical studies to evaluate the cyclic behaviour of Circular Reinforced Concrete column Steel beam (CRCS) connections. Two 3/4-scale CRCS specimens are tested under quasi-static reversed cyclic loading. Specimens were strengthened with a tube plate (TP) and a steel doubler plate (SDP). Furthermore; nine interior beam-through type RCS connections are simulated using nonlinear three-dimensional finite element method using ABAQUS software and are verified with experimental results. The results revealed that using the TP improves the performance of the panel zone by providing better confinement to the concrete. Utilizing the TP at the panel zone may absorb and distribute stress in this region. Results demonstrate that TP can be used instead of SDP. Test records indicate that specimens with TP, with and without SDP maintained their maximum strength up to 4% drift angle, satisfying the recommendation given by AISC341-2016 for composite special moment-resisting frames.

Keywords: RCS connection; composite structures; tube plate; steel doubler plate; finite element method (FEM)

1. Introduction

Utilization of composite systems has made a revolution in the construction industry, especially in constructing of tall buildings. A composite system benefits the advantages of both concrete and steel materials. The reinforced concrete columns usually are stiffer than steel columns due to larger cross sections, which could be beneficial in tall buildings where the structure's stiffness governs the design. Also, due to the nature of the concrete material and crack formations, concrete columns have higher damping capacity. Combination of steel beam and concrete column can help the designer to design larger beam spans. Concrete columns have better fire resistance, and regarding constructability, there is no need for welding and bolting at beam-column connections that speeds up the construction.

One type of the structural composite systems is called RCS (reinforced concrete column steel beam). The RCS moment frames became common in the Japan and United States in the late 1970s and early 1980s. Many experimental research have done for investigating the performance of RCS connections. Sheikh *et al*. (1989) performed seventeen 2/3 scale interior RCS connections at University of Texas and in 1993, nineteen RCS connections have been tested by Kanno (1993) at Cornell University. They studied different parameters in their tests. Parra-Montesinos (Parra-Montesinos and Wight 2001) reviewed some significant researches in this field. Kuramoto and Nishiyama (Nishiyama *et al*. 2004) studied various joint specimens and provided some proposals for increasing the shear strength of RCS connections.

Alizadeh *et al*. (2013), some suggested joint details were simulated using verified FEM to investigate the performance of the steel band plates, FBP, wide face bearing plates (WFBP), ABPs and steel doubler plates (SDP). The results showed that the performance of models depends on connection detailing, the effectiveness of the shear keys, and the level of confinement provided for the joint region.

In another research conducted by Alizadeh *et al*. (2015) scrutinized the cyclic behaviour of RCS connections. In their studies, two interior connections are investigated under reversed cyclic loading. One of the specimens had a new proposed joint detail that consisted of additional bearing plates. Comparing the performance of two specimens proved that using additional bearing plates, increases the bearing and shear strength of the joint. Furthermore, a modified method for modeling this type of connections was introduced via the use of OpenSees software.

Men *et al*. (2015a) conducted experimental studies on the behavior of RCS connection subjected to the cyclic loading. Six composite reinforced concrete column-to-steel beam interior joints were tested to study the failure mode and behavior of panel zone. The results show that end plates, band plates, cover plates and X shape reinforcement have much effect on the strength capacity of the connection.

A series of test was performed on RCS frame with two-

∗Corresponding author, Associate Professor,
E-mail: n.attari@bhrc.ac.ir
[a] Associate Professor, E-mail: nikkhoo@usc.ac.ir
[b] Ph.D. Candidate, E-mail: R.jafari@usc.ac.ir
[c] Ph.D. Candidate,
E-mail: Saeid.Alizadeh@pg.canterbury.ac.nz

ISSN: 1229-9367 (Print), 1598-6233 (Online)

bay and two-story by Men *et al*. (2015b). The results denoted that composite RCS frame systems perform satisfactorily under simulated earthquake action, which further validates the reliability of this innovative system.

Ghods *et al*. (2016) numerically investigated the mechanical behavior and failure mechanism of RCS connections to scrutinize the effect of the steel shear wall and the bracing system on mechanical behavior and ultimate resistance of frame under the seismic loading. Numerical results proved that the linear stiffness of models with X bracing and steel shear wall increase ultimate strength about three times rather than other RCS frames.

Nguyen *et al*. (2017) explored the seismic performance of a new type of RCS connation. The test results illustrated that the RCS moment frame had good ductility and energy dissipation capacity.

Some other research programs on composite connections were conducted by other researchers such as Thai *et al*. (2017), and Zhang *et al*. (2017).

There are many type of research on the performance of RCS connections with different joint details; however, only a few of them has focused on the behavior of the TP in the RCS joints. Therefore, the performance of the TP and its effects on the joint shear stiffness and strength is not well recognized. This investigation aims to clarify the influence of SDP and TP on the performance of RCS connections. In this study program, two 3/4-scale interior beam-through type RCS connections are tested under quasi-static reversed cyclic loading pattern. The experimental results are verified via the finite element models employing ABAQUS software. Furthermore; a complete FEM scrutinize is conducted to examine the performance of various types of joint details in combination with TP and SDP.

Table 1 Types and details of specimens

Models	Joint detail		Steel beam (mm)	f_c (MPa)
	SDP*	TP*		
Specimens 1	✓	✓	IPE300 +2PL2000*150*10	58.3
Specimens 2		✓	IPE300 +2PL2000*150*10	58.3

* SDP: Steel Doubler Plate, TP: Tube Plate

2. Experimental program

2.1 Specimens & material properties

The test specimens were selected from a base model with a 4-storey perimeter moment resisting frame. The connections were designed based on ASCE1994 guideline (1994), and its modifications by Cordova and Deierlein (2005). The primary design philosophy of the connection was based on the strong column-weak beam criteria that caused to use IPE 300 steel member as a beam. For postponing fracture and studying connection area, reinforced plate was welded on the IPE 300 and the beam capacity was increased, which caused the connection enter to nonlinear behavior before failure in the beam. All test specimens consisted of 3 m-long columns with 500 mm diameter circular cross-section. Columns were reinforced with sixteen φ20 steel bars (ASTM A615 grade-75) (2012) longitudinally and φ10 bars (ASTM A615 grade-60) (2012) were used for the column spirals. IPE 300 steel sections (ASTM A572 grade-50) (2012) with 3.9 m length were considered for the beams. In both specimens, steel beams were strengthened by welding two 10 mm thickness plates to the top and bottom flanges, for increasing the connection demand. The plate dimensions are presented in Table 1. At the connection of the first specimen, tube plate was used in addition to the steel doubler plate that it was welded to the beam web, and in the second specimen, tube plate was used lonely. The Self-Consolidating Concrete (SCC) was used for the column and panel zone. The nominal compressive strength of the concrete was measured 58.3 MPa. The

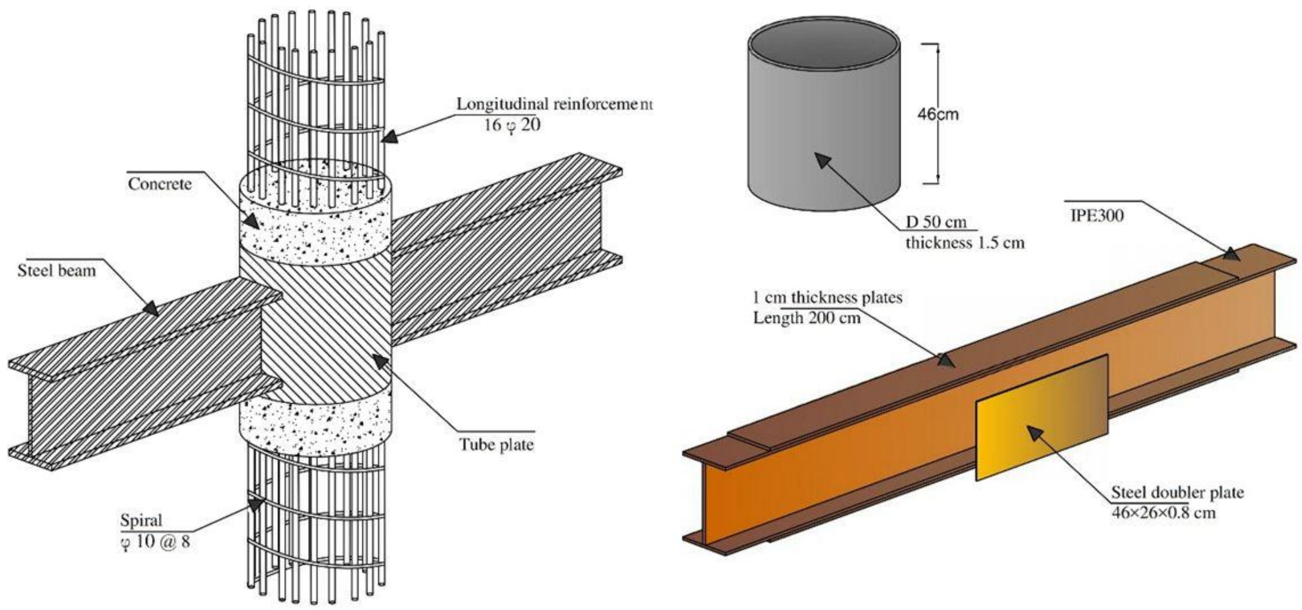

Fig. 1 Details of the specimens

Table 2 Mechanical properties of steel materials

Test spec	Type	Yield strength (MPa)	Tensile strength (MPa)	Elongation (%)
1-2	Beam	397	482	31
1-2	Tube plate	328	466	34.5
1	Steel doubler plate	338	464	17
1-2	Longitudinal reinforcement	447	701	23.5
1-2	Spirals	404	638	28

details of these specimens are shown in Table 1 and Fig. 1 as well. The mechanical properties of the steel materials resulting from tensile tests are demonstrated in Table 2.

2.2 Test set up

The pinned connection was used at the lower end of the column and roller supports were embedded at the beam ends. The roller support allowed free translational movement and rotation in the direction of the lateral loading. The beams and column's ends were braced laterally to restrain the out-of-plane movements of specimen during the tests. Cyclic lateral displacements were applied using two 500 KN compression actuators at each side of the column. Four post tension rods were used to apply an axial compression force to the column. These rods connected two plates at the bottom and top of the column. Axial loading that can be applied with the instrumentation available was 400 kN. A 400 kN axial compression force was applied to the concrete column at the beginning of the test, which was about 4% of the column's gross axial strength; this force is checked by the load cell during the

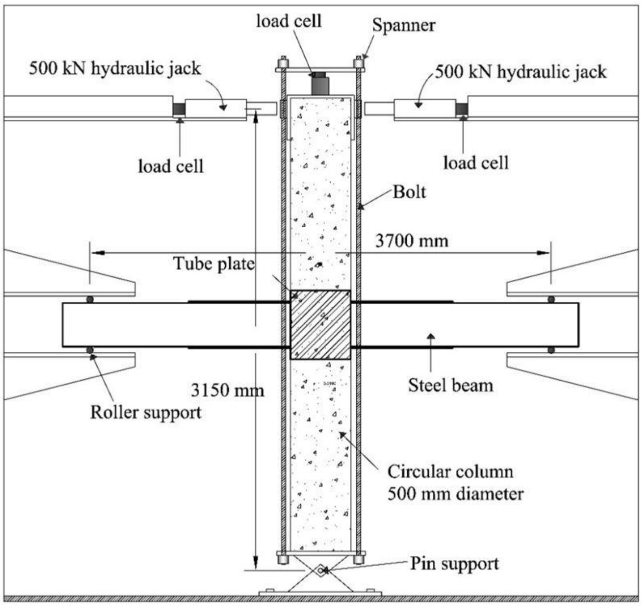

(a) Schematic configuration

(b) Test specimen

Fig. 2 Test setup

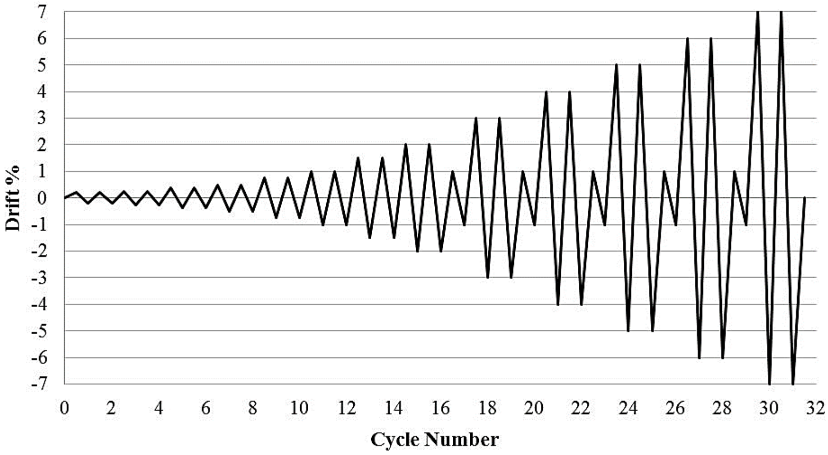

Fig. 3 Loading pattern

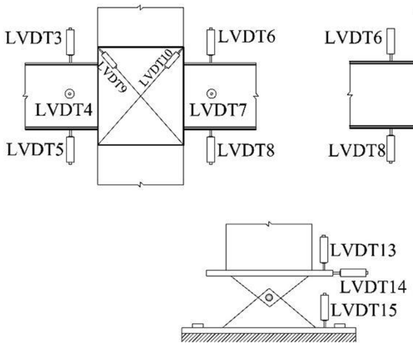

(a) Location of LVDTs

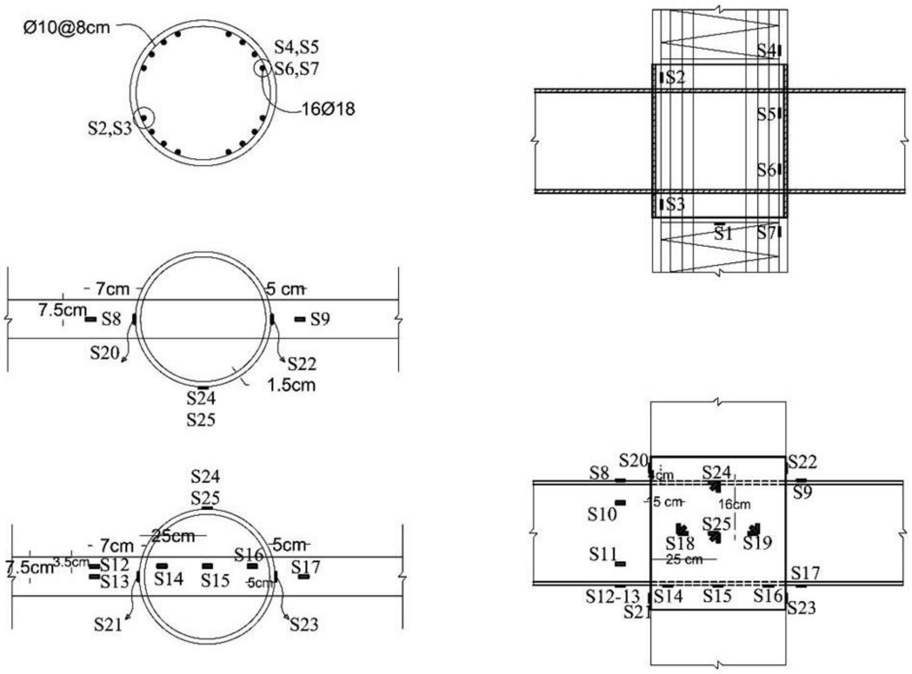

(b) Location of strain gauges

Fig. 4 Location of LVDTs and strain gauges

test. The column's gross axial strength is the concrete compression strength multiplied by total column Area according to ACI318. Load variation was not high during loading but in the large displacements, it was controlled by loosening and tightening the bolts. The cyclic loads were applied using the horizontal jacks.

Table 3 Test results

Specimen	Loading direction	P_y (N)	Δ_y (mm)	P_{max} (N)	Δ_{max} (mm)	P_u (N)	Δ_u (mm)	μ (Δ_u/Δ_y)
1	Positive	273310	49.67	320640	105.6	246528	165.3	3.32
	Negative	273302	49.64	310880	105.5	248704	160.1	3.31
2	Positive	220100	49.67	310560	115.2	248004	157.8	3.18
	Negative	220082	49.61	309600	96.4	247680	134.1	2.70

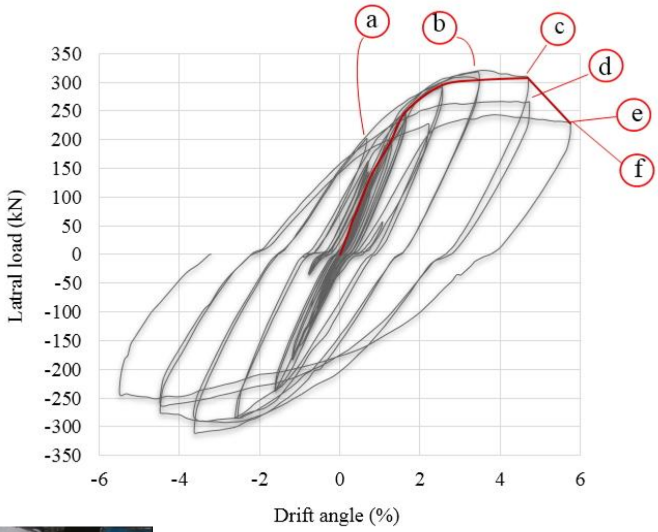

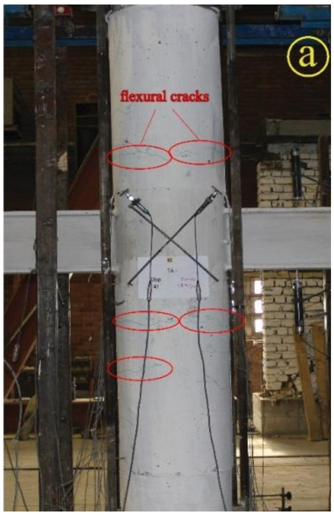

(a) Cracks on the column at about 1.5% storey drift

(b) Beam yielded at about 4% storey drift

(c) Buckling of beam flange at about 5% storey drift

(d) Buckling of beam web at about 5% storey drift

Fig. 5 Specimen 1 Lateral load response at deferent storey drift

(e) Complete buckling of about 6% storey drift

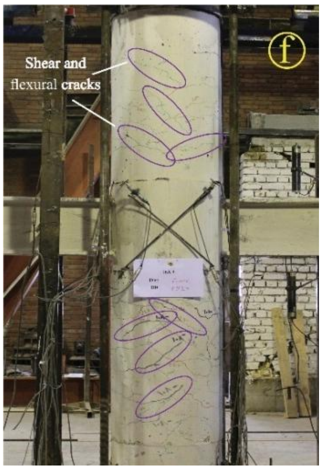

(f) Cracks on the column at about 6% storey drift

Fig. 5 Continued

2.3 Loading pattern

The cyclic displacements are applied in 28 cycles starting with a 0.2% drift angle and maintaining 0.25%, 0.375%, 0.5%, 0.75%, 1%, 1.5%, 2%, 3%, 4%, 5% and 6% drift angles, which is shown in Fig. 3. Based on the drift angles, each cycle was repeated twice in this loading protocol. Two load cells were set between the hydraulic jacks and the column tip on each side of the column to record the lateral loads.

2.4 Instrumentations

Column top end displacements were recorded by employing two displacement transducers placed at the top of the column in the loading direction. Also, fifteen LVDTs (Linear Variable Differential Transformers) were installed on the beam, at the panel zone, and at the tube plate to record the rotations and distortions. Strain gauges were used to monitor the strains in the beam, tube plate, reinforcement, and spirals. The arrangement of the beam strain gauges was concentrated at the beam near the tube plate. The layout of the strain gauges and the displacement transducers is presented in Fig. 4.

3. Experimental results

3.1 Test observations

The experimental results and the main parameters which characterize the behavior of the specimens are illustrated in Table 3. Both specimens had a good performance, and plastic hinges occurred simultaneously in two parts of the beam, at the column face and the flanges of the beam that had not been strengthened. No inelastic deformation was found in the tube plates throughout the experiments. It was found that both specimens maintained the maximum strength at drift angles greater than 4%, satisfying the recommendation given by AISC 341-2016 (2017) for a composite special moment-resisting frame. All displacement values are modified considering the displacement of the support.

3.1.1 Specimen 1

Load versus storey drift responses of the specimen 1 is plotted in Fig. 5, which proves that specimen 1 has demonstrated ductile behavior and good energy dissipation capacity.

At point "b", the beam is yielded at two sections, at the

Fig. 6 Weld fracture on specimen 1 at 5% storey drift

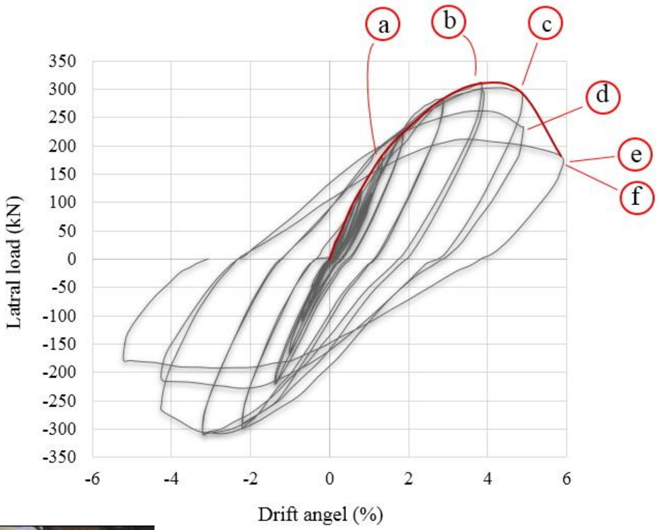

(a) Cracks on the column at about 1.5% storey drift

(b) Beam yielded at about 4% storey drift

(c) Buckling of beam flange at about 5% storey drift

(d) Buckling of beam web at about 5% storey drift

Fig. 7 Specimen 2 Lateral load response at deferent storey drift

flange and web near the tube plate, and where the added plate of the beam is finished. At point “c”, the weld of the reinforcement plate fractured due to the local buckling of beam flange. The local buckling of the beam has become more intense at point “d”, causing the beam web to buckle. Furthermore, the flange of the beam was buckled near the tube plate. Eventually, at point “e”, the beam was completely buckled, and the hysteretic curve showed more than 20% decrease from maximum load capacity, which stopped the test.

Fig. 5 also depicts the first flexural cracks of the column, which happened at about 1.5% storey drift At point “a”. The first cracks occurred due to bending at 1.5% storey drift and after a 3% drift, shear cracks appeared. Local flange buckling in beam began at approximately 4% storey drift, and yielding was observed at 750 mm from the tube plate. The weld fracture occurred at the flange of the added plate on the beam at about 5 % storey drift. Web buckling was also observed at this drift angle.

(e) Complete buckling of about 6% storey drift

(f) Cracks on the column at about 6% storey drift

Fig. 7 Continued

During the second cycle of about 5% storey drift, a distinct fracture on the flange was apparent. This rupture eventually propagated through the full flange width. The fracture of the specimen 1 demonstrated in Fig. 6. Because of web buckling, the strength of the specimen reduced by about 20% of the peak strength.

3.1.2 Specimen 2

The behavior of specimen 2 was almost the same as the specimen 1. The only difference was that softer behavior observed in this specimen due to the absence of the steel doubler plate. All failure mechanisms and cracking pattern that happened in specimen 2 were observed similar to that of specimen 1. In this specimen absence of the SDP has decreased the yielding strength a little but it does not affect the ultimate strength, on the other hand; the descending chart showed a sharp drop in comparison with specimen 1. The main difference failure in this specimen was that the web of beam was yielded on the panel zone at the first time, then the flange of the beam is yielded. The cracking patterns of columns and beam are illustrated in Fig. 7.

3.2 Stiffness & energy dissipation capacity

Stiffness retaining capacity of the tested specimens was investigated by analyzing lateral peak-to-peak stiffness at each cycle. The stiffness of each cycle is normalized by the stiffness of 1% storey drift in Fig. 8 that are $K1_{SP1}$ = 492.75 kN/m and $K1_{SP2}$ = 460.5 kN/m for specimens 1 and 2 respectively. The dissipated energy during each cycle of lateral loading is illustrated in Fig. 9 considering the area under load-deformation loops. Up to 1.5% drift, the dissipated energy of both specimens is the same because the cracks of concrete did not start and the column elastic capacity is more than yielding of the beam. The initial stiffness of both specimens is similar which demonstrates that SDP has a small effect on the initial stiffness and as shown in Fig. 8, it’s effect on normalized stiffness is also negligible that proves SDP does not affect the rigidity of the connection in elastic zone.

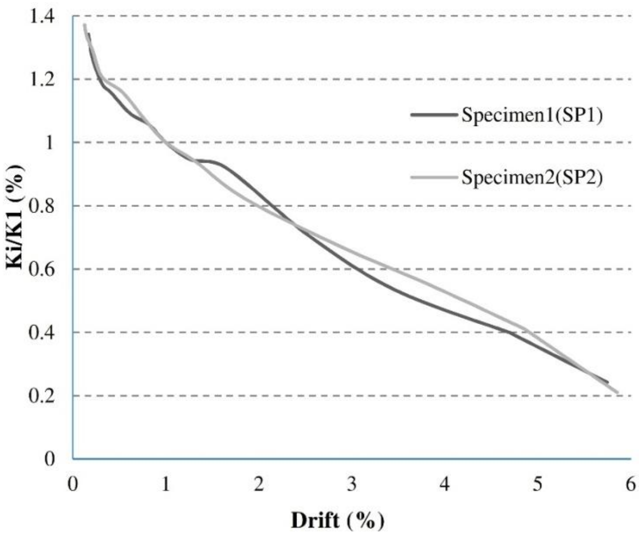

Fig 8 Normalized lateral stiffness

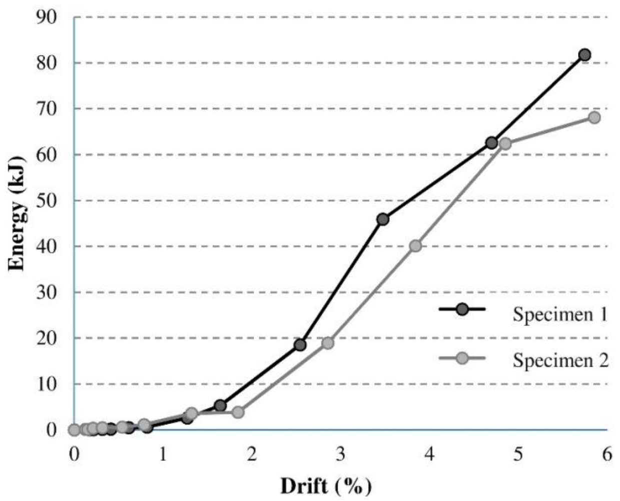

Fig. 9 Dissipated energy

3.3 Behavior of the beam plastic hinges

As indicated in Figs. 5 and 7, plastic hinges were formed in the beam of both specimens, approximately at 750 mm distance from the column face. In both specimens, yielding was seen at the web of the beam. The imposed bending moments to the tube plate were 409 and 397 kN-m for first and second specimens, respectively.

Strains versus storey drift of the beams for both specimens are presented in Fig. 10. As it could be inferred, in the specimen 1; due to the presence of the steel doubler plate on the web of the beam in the panel zone, more force was absorbed by the beam in the panel zone, and this has caused the energy absorption by the beam in specimen 1 to be more than that in specimen 2. However, yielding occurred with more intensity on the web of the beam of the specimen 2 due to lack of the steel doubler plate.

The strain of the steel beam flange of specimen 1 was about 1.5 times greater than specimen 2 which caused flange distortion in specimen 1 near the column faces as displayed in Figs. 10 and 11. This proves more energy is absorbed by the beam of specimen 1, but in specimen 2, the force is transferred to other parts, including tube plate, which takes advantage of the maximum capacity of each part.

The results which are shown in Fig. 10(c) demonstrate that the forces transferred to TP in specimen 2 are more than 2 times of specimen 1 due to lack of SDP.

3.4 Behaviour of the tube plate

Tube plate Behaviour was observed by four uniaxial and two rosette strain gauges. Strain gauges number 20 to 25 were placed to measure the strain on the tube plate as depicted in Fig. 4. According to Figs. 5, 7 and 11, no sign of yielding in the tube plate could be detected. This proves the high performance of the connection in limiting tube's rotation. The tube plate's role is to provide confinement to the concrete in the panel zone; also, one part of the load acting on the panel zone is transferred to the column through tube plate, therefore beam plastic hinge happens at larger drift. The strains are indicated in Fig. 12.

3.5 The behavior of the panel zone

As illustrated in Fig. 4, LVDTs were set at the panel zone to record the shear deformations. Equation 1 was used to obtain the shear deformations. In these equations, L_3 & L_4 are the lengths of LVDTs, and L_1& L_2 are the TP dimensions; which are shown in Fig. 13.

Figs. 13(a) and (b) presents the effects of removing the SDP on the shear deformations of panel zone in the specimen with TP. This figure demonstrates that eliminating SDP causes the TP capacity be used.

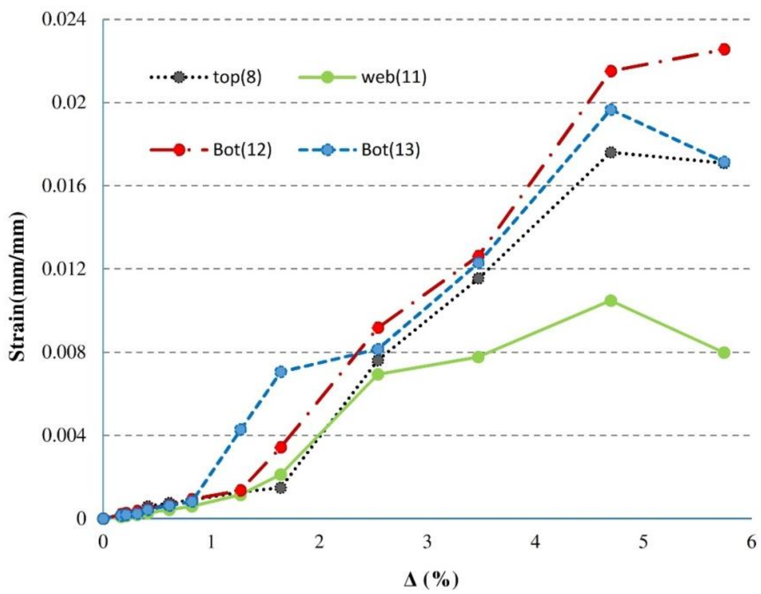

(a) Specimen 1

Fig. 10 Strain of the steel beam web and flanges versus storey drift

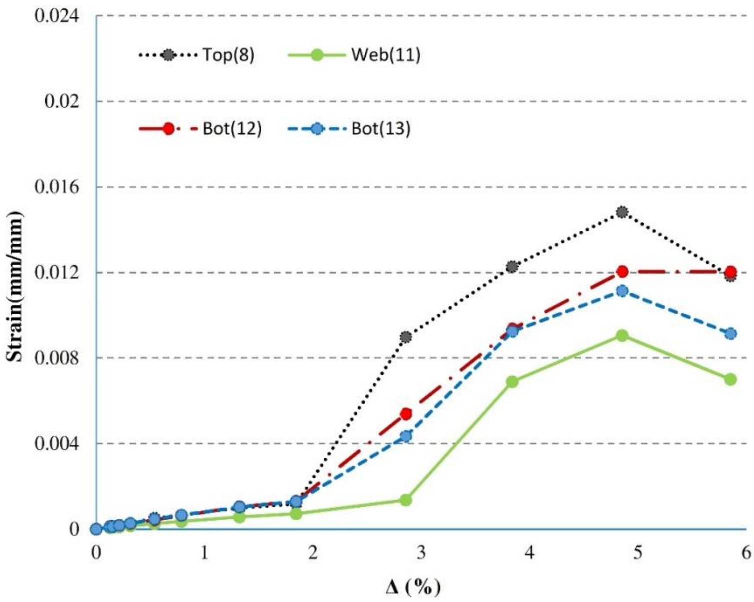

(b) Specimen 2

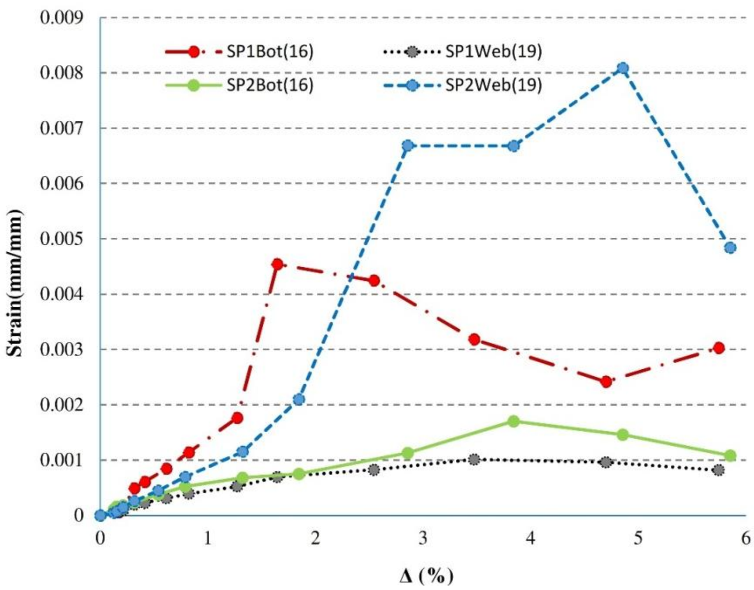

(c) In the panel zone

Fig. 10 Continued

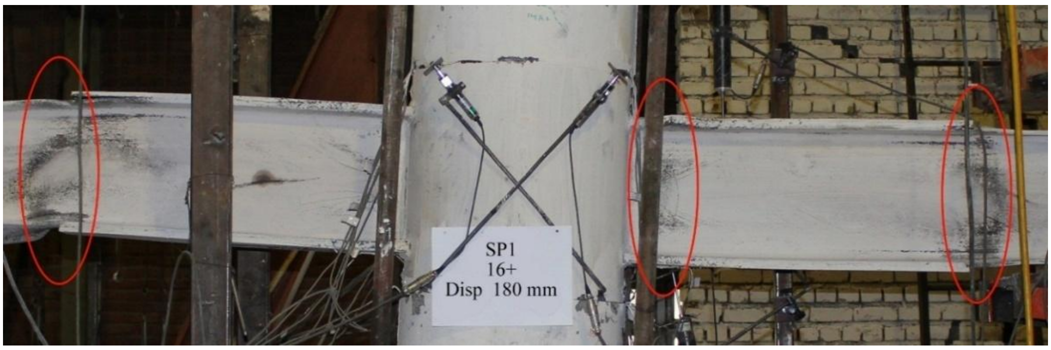

Fig. 11 Local buckling of the beam for specimen 1

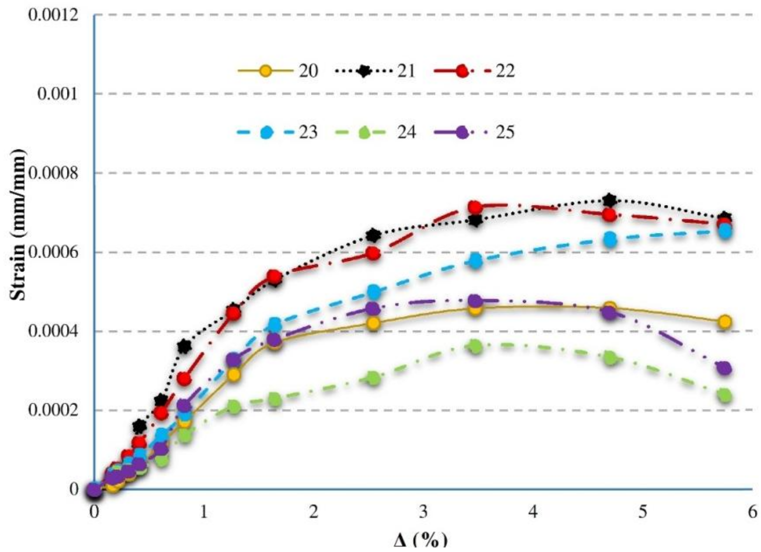

(a) Specimen 1

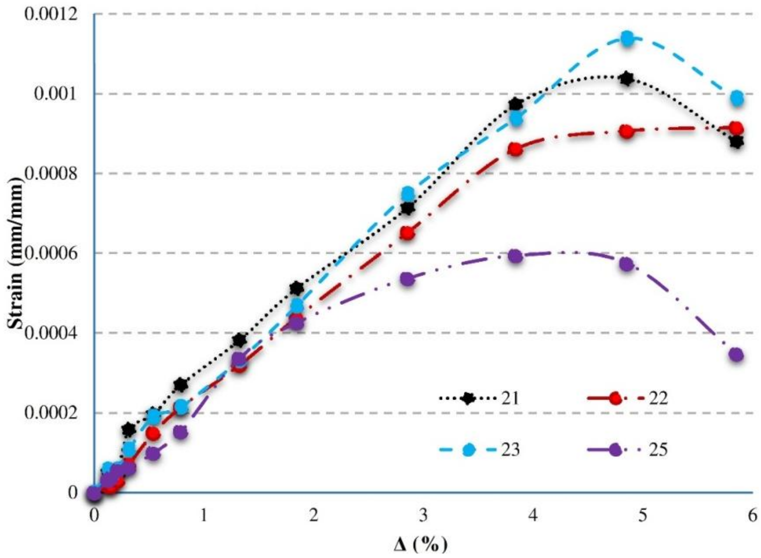

(b) Specimen 2

Fig. 11 Strains of tube plate versus storey drift

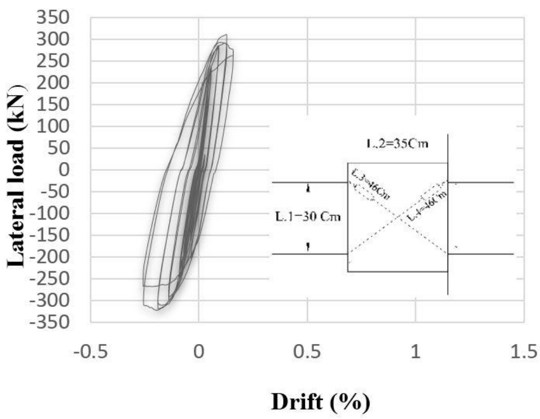

(a) Specimen 1

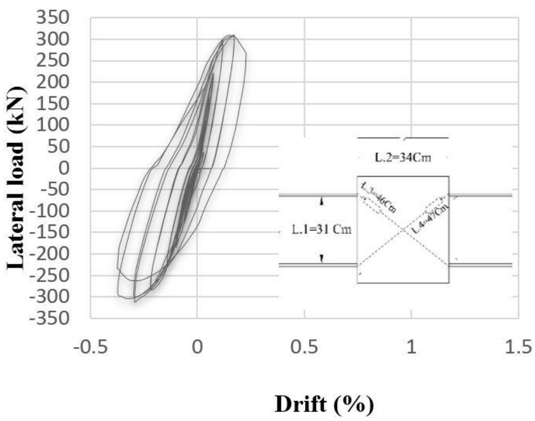

(b) Specimen 2

Fig. 13 Shear deformations of panel zone

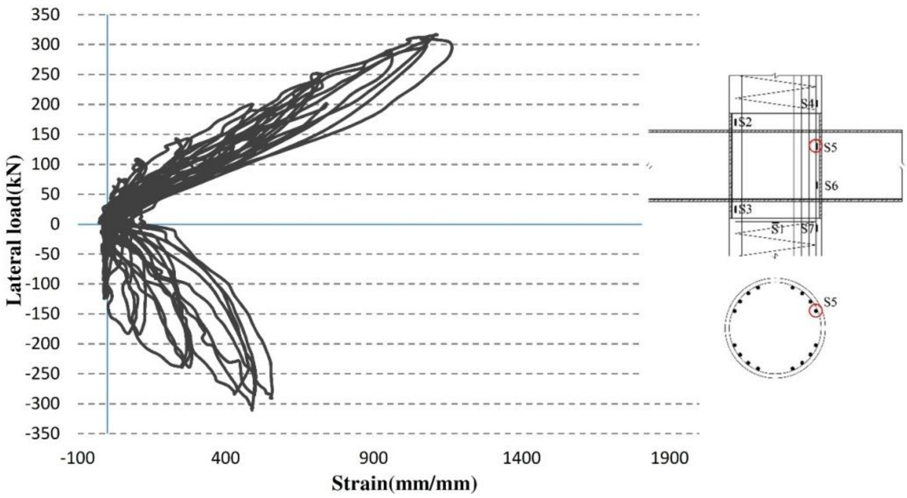

(a) Specimen 1

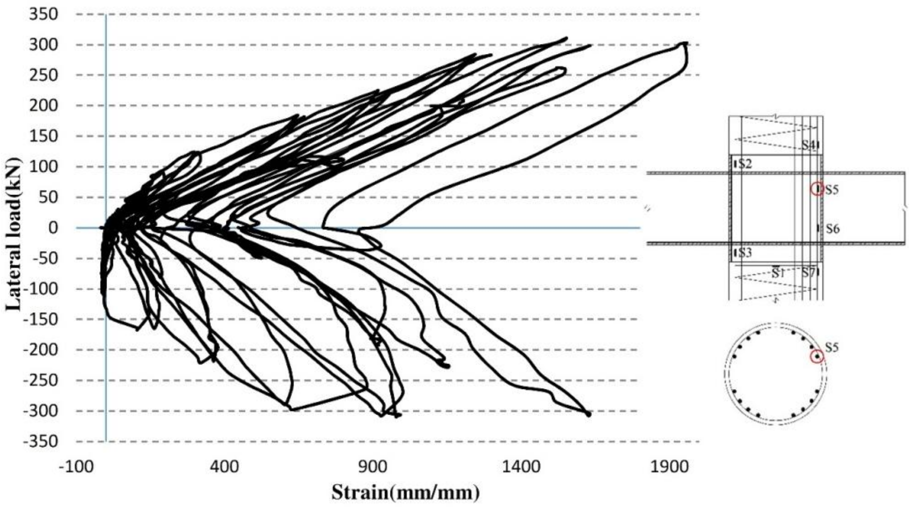

(b) Specimen 2

Fig. 14 Strains of the column reinforcements

$$\gamma_1 = \frac{\pi}{2} - \cos^{-1}\left(\frac{L_1^2 + L_2^2 - L_3^2}{2L_1L_2}\right)$$

$$\gamma_2 = -\frac{\pi}{2} + \cos^{-1}\left(\frac{L_1^2 + L_2^2 - L_4^2}{2L_1L_2}\right) \qquad (1)$$

$$\gamma = \frac{\gamma_1 + \gamma_2}{2}$$

3.6 Behaviour of the column reinforcements and spiral

A number of strain gauges was used to obtain the strains of the reinforcements in different parts of the panel zone as shown earlier in Fig. 4. Strains of different reinforcements in the hysteretic loop have been indicated in Figs. 14(a) and (b) and the strains of the column reinforcements and spiral versus storey drift for specimen 1 and 2, are illustrated in Figs. 15(a) and (b). The beam of specimen 1 has an SDP, and because of that, the concentration of force in the beam is more than specimen 2. Thus, more loads are transferred to the column, and the strains of column's reinforcements are higher in these specimens because of more demand. The forces of the panel zone divided by tube plate, web of beam and concrete core. Given that part of the force of the connection area is tolerated by the web, the excess force should be transferred between the other two sections, and therefore the forces in the specimen 2 are greater than the first one.

4. Finite element modeling

The experimental specimens were modeled using ABAQUS software (2010). All of the specimens details, materials, boundary conditions and interactions were considered based on the experimental program. To decrease the computational time, half of the specimens were modeled, using the symmetrical situation at the centre of the specimens. Since there is no significant nonlinear behavior at the end part of the columns and beams, these regions were modeled by one-dimensional beam elements.

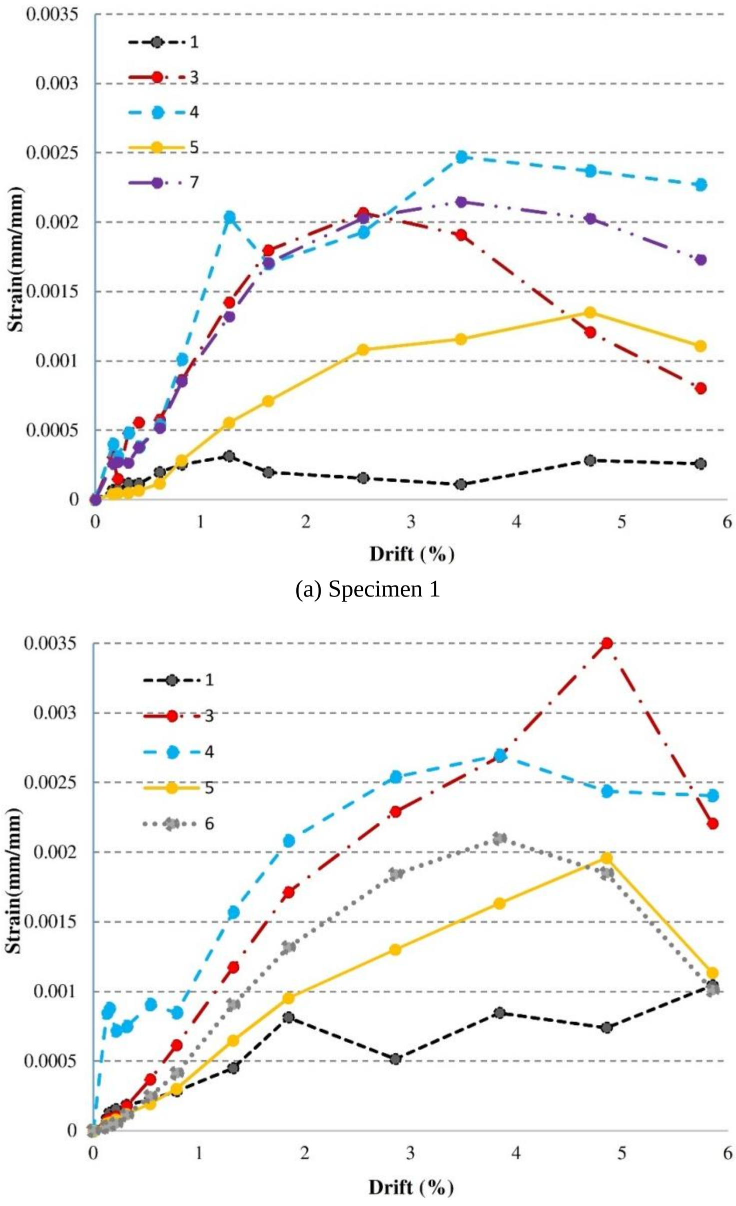

(a) Specimen 1

(b) Specimen 2

Fig. 15 Strains of the column reinforcements versus storey drift

Because modeling the whole beam and column cause a lot of calculation time and studying the connection behavior is the purpose of this research, the end part of it is modeled with nonlinear beam and in Fig. 15, the result is compared with the situation that whole beam and column is modeled with solid elements. The simplified model was controled by a full three-dimensional one, and no significant difference was observed.

The concrete damage plasticity-based damage model is considered for concrete assuming the tensile cracking and compressive crushing of the concrete material as the main failure mechanisms. Parameters, which are needed in this material model, are obtained from CEB-FIP model code 90 (1990), based on the concrete compressive strength. The nonlinear behavior of steel beams and reinforcement bars were simulated using von Mises yield criterion with isotropic hardening. subsequent a short checking about several model, the 15 mm mesh size was found adequate for modeling. The result of uniaxial tension tests is used for defining the stress-strain relationship of the steel beams.

The 8–node solid elements, which are known as C3D8R elements in ABAQUS software, are utilized for modeling steel beams and concrete columns. The reinforcements are modeled using one-dimensional two nodes truss elements (T3D2) and are fully embedded in concrete. These assumptions are used for simplifying the finite element models. Separation of steel beam and concrete column at the joint region was allowed during the analysis for better simulation of the interaction between the concrete and steel. The models are analyzed in two steps, at first, the axial force of column is applied, and then the column is pushed laterally up to 5% storey drift.

The backbone curve is plotted according to ASCE41-17 (2017), and FEM results of both specimens are observed to

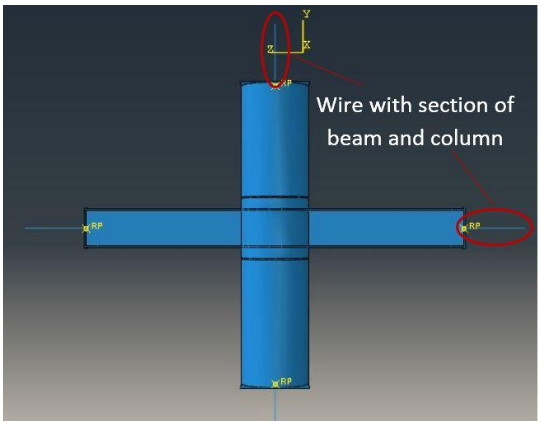

Our study model with 2 Cm mesh

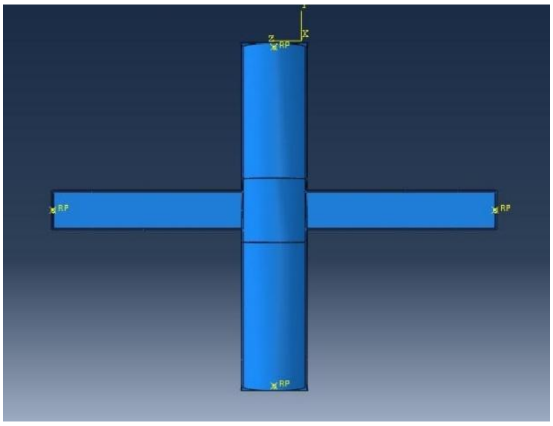

Fully model with 2 Cm mesh

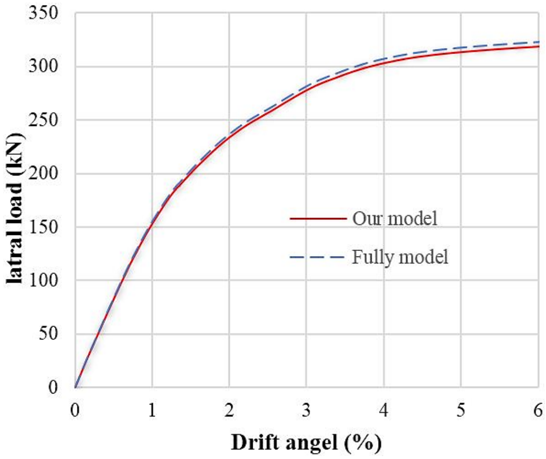

Fig. 16 Our model compare with fully model

have a good conformity with the experimental ones and the analytical load-deflection relationships. Furthermore, as could be seen in Fig. 17, the load–storey drift response of FEM analysis results and the overall crack pattern of FEM model are similar to the experimental results. Also, diagram of 2 line drawed base on Idealized Force–Displacement Curve for NSP in ASCE 41-17.

4.2 Case study

4.2.1 Simulated models

Nine interior beam-through type RCS connections are investigated numerically in this study. Several joint details are simulated using the verified model to investigate the effects of TP, face bearing plate (FBP), Band Plate (BP) and steel doubler plates behavior in RCS connections. Simulated models are grouped into three main categories to ensure that all the possible failure modes are captured. Each of these categories consists of models with and without TP and SDP.

All of the models consist of 3000 mm-long concrete column, with 500 mm diameter circular cross-section. Columns are reinforced with sixteen Φ20 steel bars. Φ10 bars are used for joint and column stirrups. IPE 300 steel sections with 3900 mm length are considered for the beams. In three models, the thickness of the steel beams flanges is increased to 20 mm, for imposing larger forces to the panel zone. These models are specified by adding “(s)” after the model name. In three models, the flanges of steel beams are increased to 25 mm. These models are named by adding “(ss)” after the model name.

In the joint region of different models, steel doubler plates, steel band plates, and TP are used according to table 4.

4.2.2 Load-storey drift

The load-storey drift responses of simulated models are indicated in Fig. 18(a) to compare the performance of S-T, T, and F-B-S. As it is shown in this figure, S-T and F-B-S have almost the same stiffness but T model has a lower stiffness, and its first yielding begins sooner, and finally, the three models have the same ultimate strength.

Fig. 18(b) displays the load-storey drift response of model T(s) and S-T(s) are almost the same, but the T(s) model has the lower yield strength. Both models capacity is more than 1.2 times of F-B-S model that proves TP has better performance than the combination of FBP and Band Plate, which improves the performance of connection, and adding SDP in models having TP did not have an important impact.

As it could be seen in Fig. 18(c), the load-storey drift response of model T(ss) is higher than models F-B-S(ss). This indicates that using TP instead of the combination of SDP, FBP and Band Plate improves the performance of the

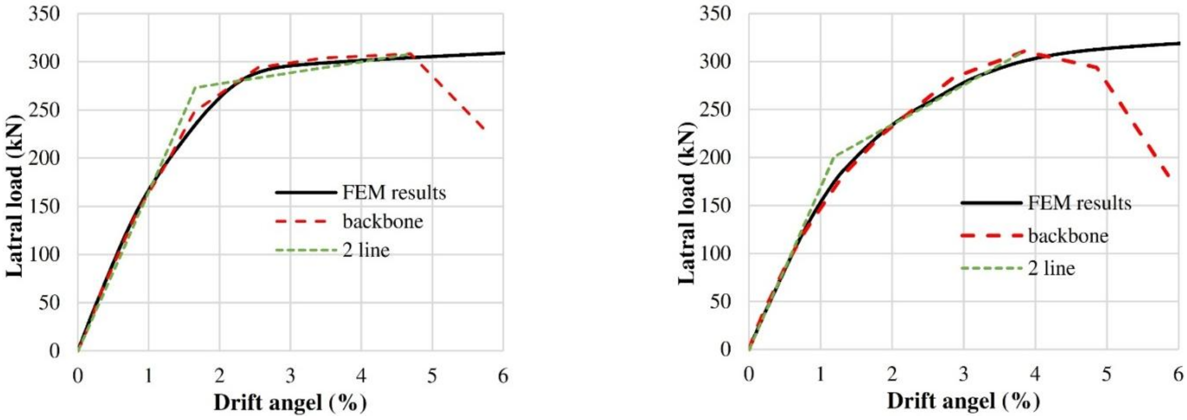

(a) Specimen 1 (b) Specimen 2

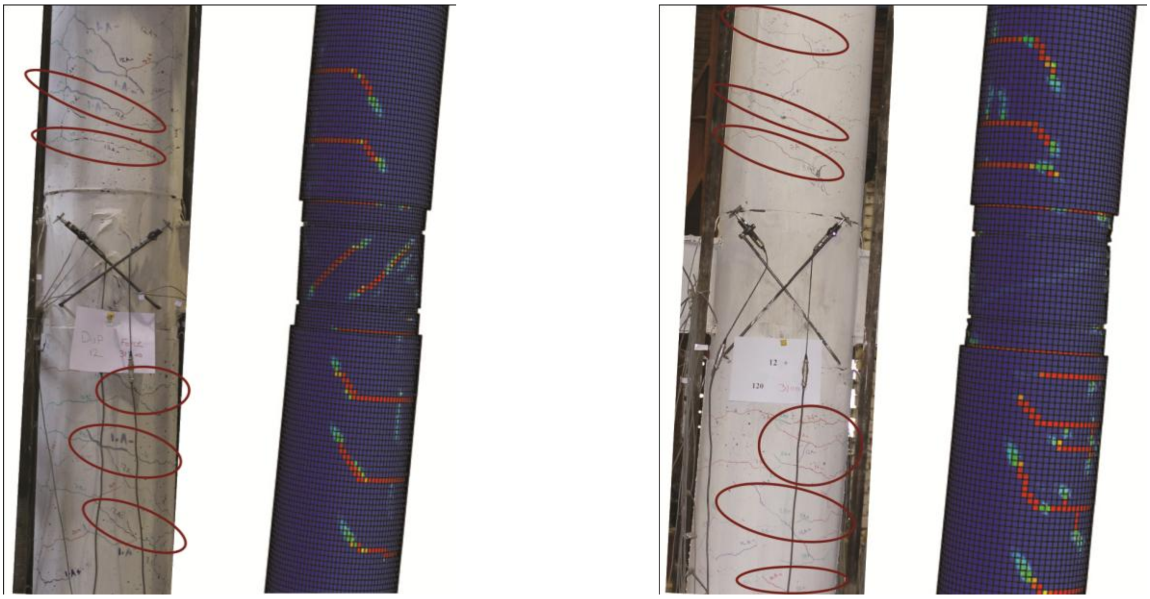

(c) Specimen 1 (d) Specimen 2

*Note: Backbone curves shall be drawn through each point of peak displacement during the first cycle

Fig. 17 Test and FEM lateral load-story drift response and crack pattern

Table 4 Joints details

Models	Joint Detail				Steel beam Flange thickness		
	FBP	BP	SDP	TP	10.7 mm (IPE 300)	20 mm	25 mm
F-B-S	✓	✓	✓		✓		
S-T			✓	✓	✓		
T				✓	✓		
S-T (s)			✓	✓		✓	
F-B-S (s)	✓	✓	✓			✓	
T (s)				✓		✓	
S-T (ss)			✓	✓			✓
F-B-S (ss)	✓	✓	✓	✓			✓
T (ss)				✓			✓

*Note: FBP: Face Bearing Plate; BP: Band Plate; SDP: Steel Doubler Plate; TP: Tube Plate; (s): 20 mm Flange Thickness, (ss): 25 mm Flange Thickness

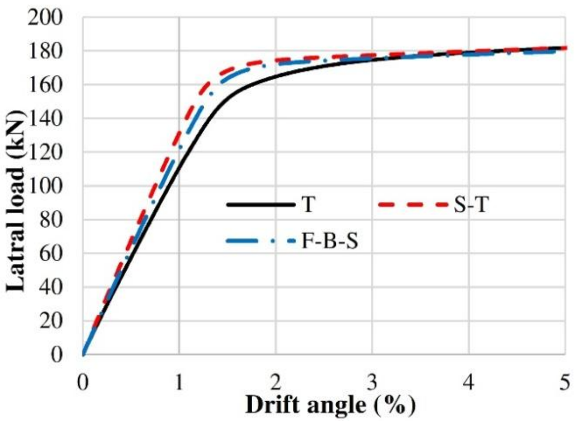

(a) T, S-T, F-B-S

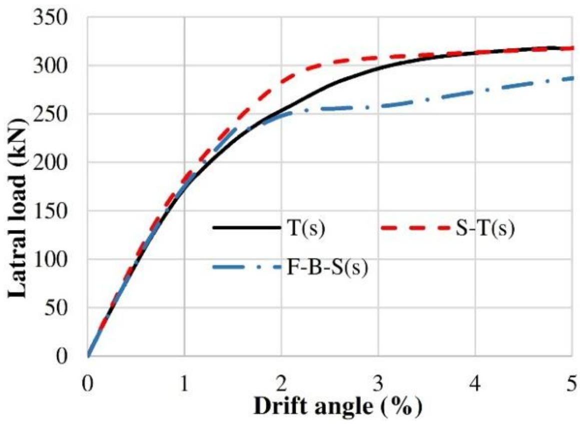

(b) T(s), S-T(s), F-B-S(s)

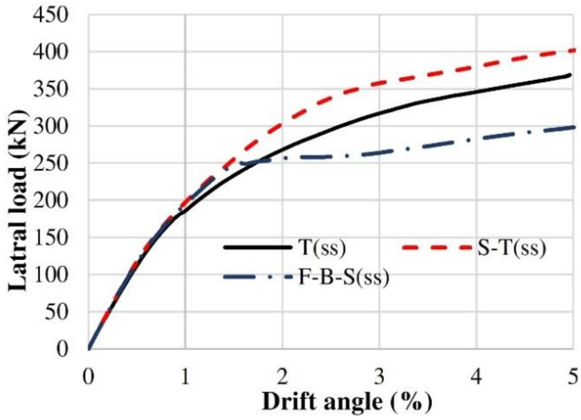

(c) T(ss), S-T(ss), F-B-S(ss)

Fig. 18 Lateral load-story drift response of models

panel zone and considering the construction difficulty. Using TP is more practical than usual connections.

With regard to the comparison of each of the three graphs in Fig. 18, it can be concluded that the use of a tube plate increases the final strength and also increases the stability of the connection that it is better than the models F-B-S. On the other hand, by comparing the S-T and T models, it can be said that the use of the tube plate without the doubler plate also shows a good behavior in all categories.

4.2.3 Cracking and failure modes

The tensile and compressive concrete damage of columns at 4% storey drift is shown in Figs. 19 and 20.

The crack pattern of the models F-B-S, T and S-T are shown in Figs. 19(a) and 20(a). It could be seen that in model F-B-S most damages in the connection area happened regarding tensional cracks due to the insufficiency of concrete confinement, but in model T and S-T cracks at the connection area reduces because TP increases the concrete confinement and differences between the crack pattern in models T and S-T are negligible. Also, Diagonal cracks of model F-B-S started at 0.75% storey drift, and in model T diagonal and flexural cracks could be observed at about 0.85% drift storey. As it could be observed, utilizing TP instead of SDP causes the cracks propagation occurs at higher storey drift.

Figs. 19(b) and 20(b) illustrate the cracking patterns of the second category of models with stronger beams than the first group. Thus, the cracks in the columns of this group are more than the first category. In this category same as the previous one, model T(s) has fewer cracks because of using TP instead of FBP and SDP, which causes better confinement in concrete at the connection area. Diagonal cracks of the column in model T(s) occurred at 0.8% storey drift, but in model F-B-S(s) diagonal cracks started at 0.7% storey drift. The columns of the third group are shown in Figs. 19(c) and 20(c) at 4% storey drift. The model with TP has the fewer cracks considering that the cracks in this category are more than other categories.

In strong beam and strong column models which failure occurs in the connection; when the TP does not exist, the concrete stress in the panel zone is increased which caused the failure in this part and reduction in the strength of the connection. In the models with TP due to increasing in the confinement and load bearing for the TP, the connection failure occurs at higher drifts, which means that models with TP have higher safety and capacity.

The Von-Misses stress contours of the beams in different models are indicated in Fig. 21. The web of the beam at the panel zone in models without tube plate tolerated a higher level of stresses. Furthermore, the efficiency of the tube plates in models T is lower than model S-T due to an absence of SDP for transferring the joint forces to the TP.

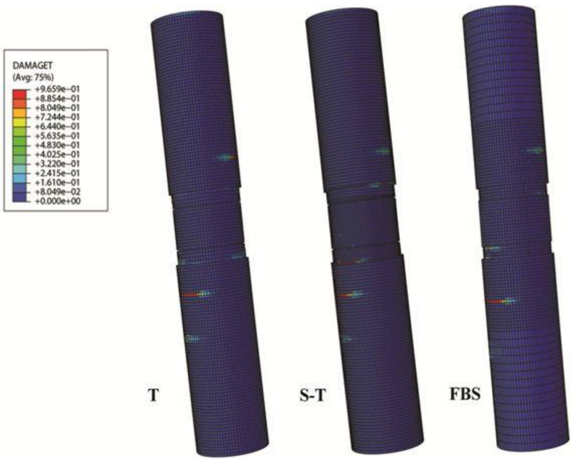

(a) Models F-B-S, C, S-T, T

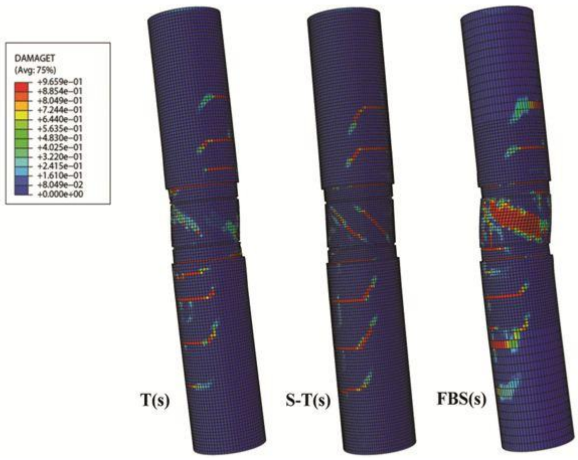

(b) Models F-B-S(s), S-T(s), T(s)

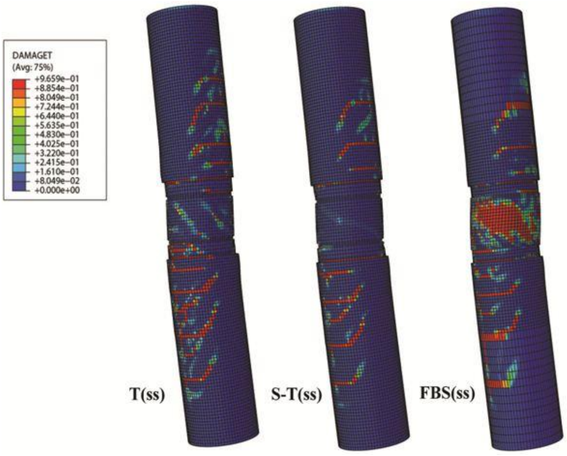

(c) Models F -B-S(ss), S-T(ss), T(ss)t

Fig. 19 Tension cracks in models at 4% story drift

In the model, F-B-S beam yielding started at about 1.13% drift and beam yielding in model T and model S-T started at 1.09% and 1.17% storey drift.

Also, beam yielding in model F-B-S(s) started from the web of the beam at 1.29% storey drift. In models T(s) and S-T(s) yielding started in the web of the beam at 1.32% and 1.43% storey drift. It could be concluded that models with TP yielding started at higher storey drift levels than models without TP. TP transfer forces to concrete properly, so stresses in flanges of the model with TP are lower than

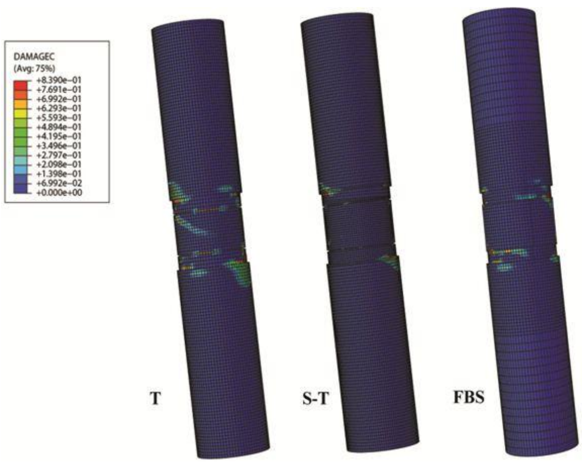

(a) Models F-B-S, C, S-T, T

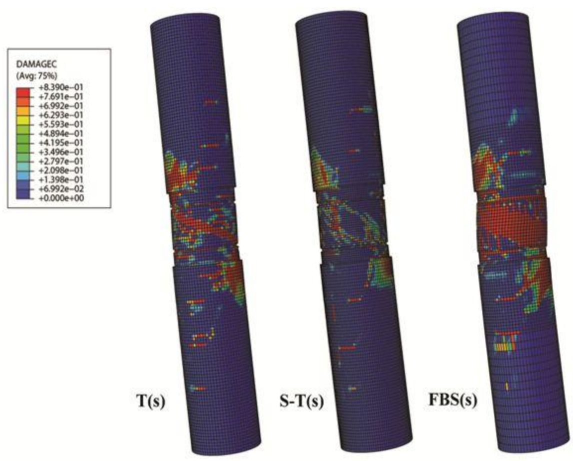

(b) Models F-B-S(s), S-T(s), T(s)

Fig. 20 Compression cracks in models at 4% story drift

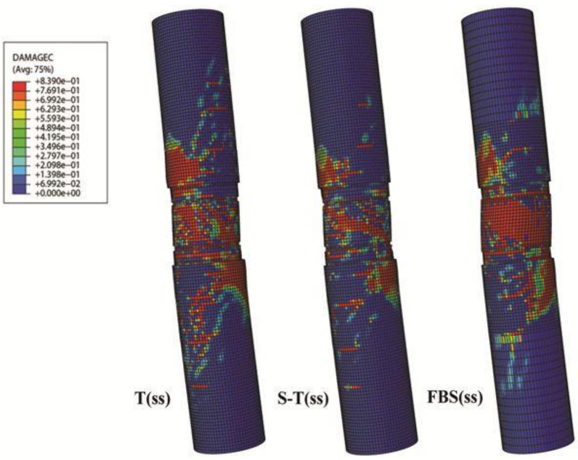

(c) Models F -B-S(ss), S-T(ss), T(ss)

Fig. 20 Continued

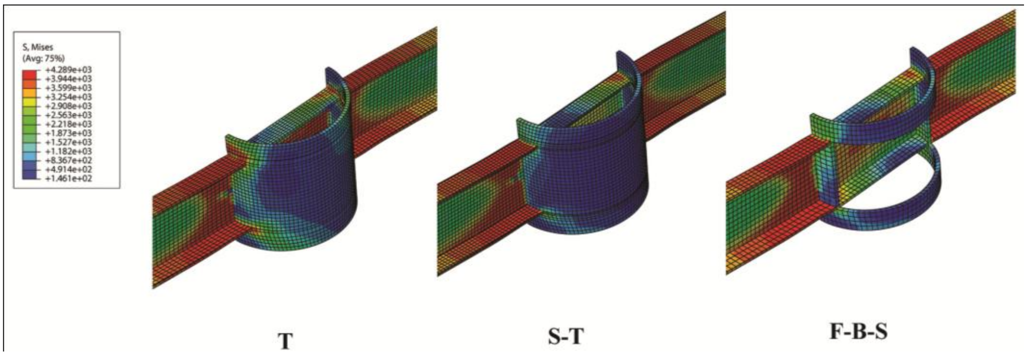

(a) Models F-B-S, C, S-T, T

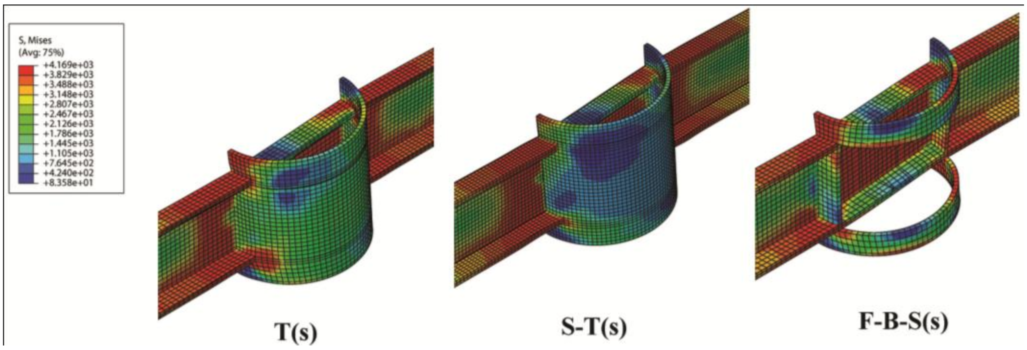

(b) Models F-B-S(s), S-T(s), T(s)

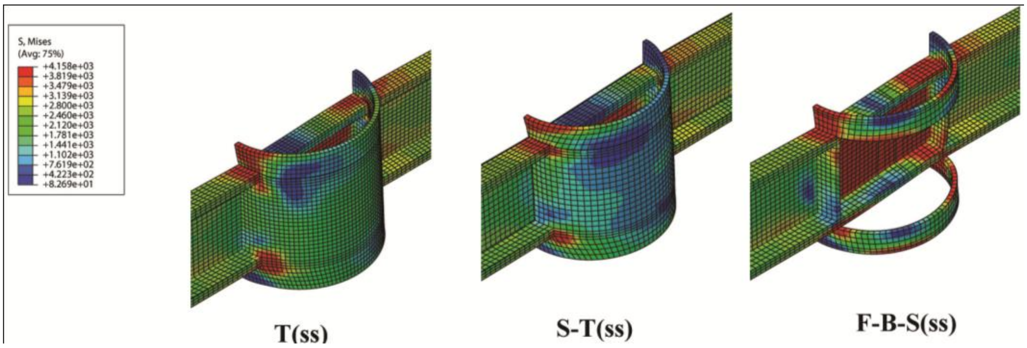

(c) Models F -B-S(ss), S-T(ss), T(ss)t

Fig. 21 Stress of beams in models at 4% story drift

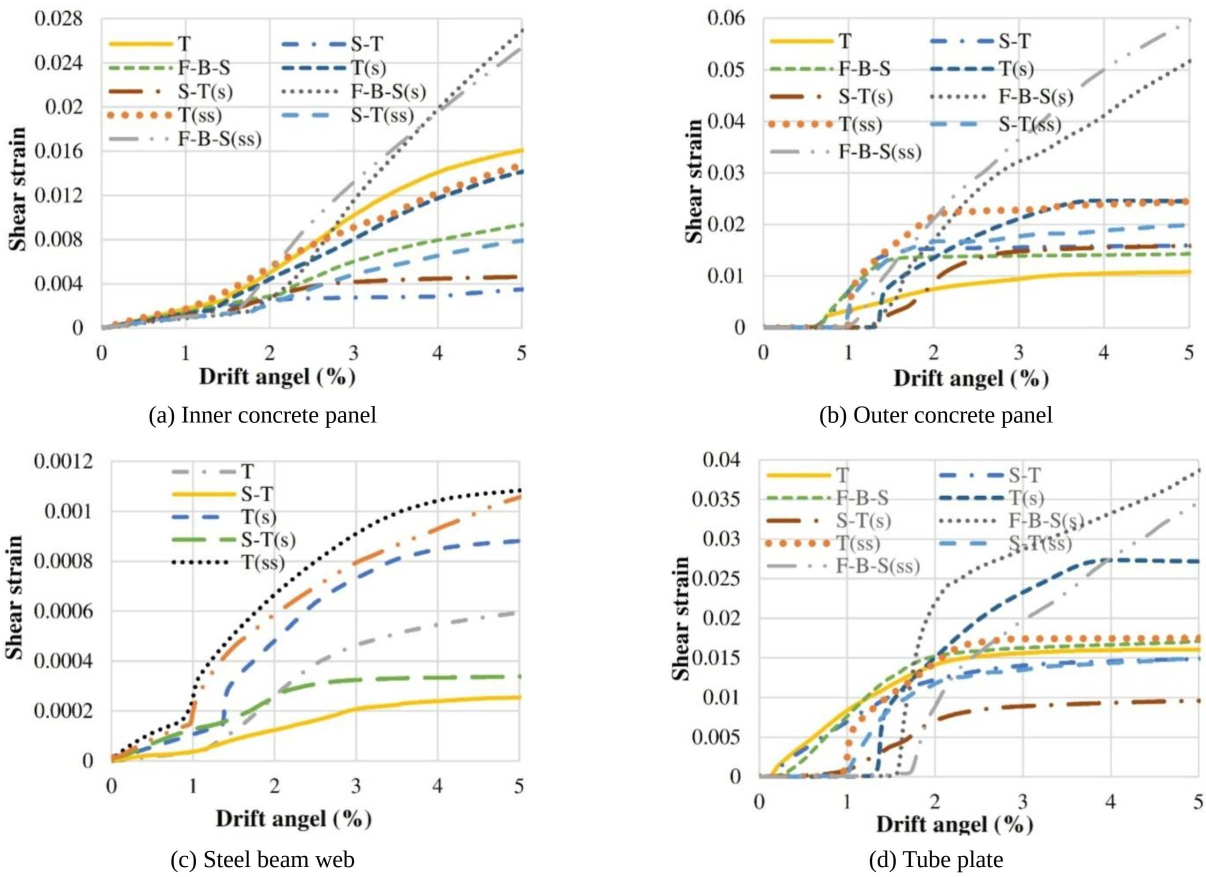

Fig. 22 Shear strain in the joint shear of models

those in model F-B-S.

In Fig. 21(c), the third group results and the distribution of stresses in models are very similar to the second group.

At 1.19% storey drift web of the steel beam in models F-B-S(ss) started to yield, Also, beam yielding in model T and S-T started at 1.18% and 1.34% storey drift.

4.2.4 Shear strain

It is important to know the load distribution in the connection. For this purpose, the shear strains of joint shear mechanisms are described in Fig. 22. The strains are extracted from the middle of steel beam web, cover plate and the inner and outer concrete panels.

The shear strains of the inner concrete panel are illustrated in Fig. 22(a). It could be perceived that shear strain increased in all of the models at about 0.6% storey drift. The shear strain of the inner concrete panel in model T is lower than model F-B-S and S-T due to using TP instead of steel doubler plate. In Fig. 22(b), due to the failing of the beam in low load and the lack of high load in the tube, all three models have the same behavior.

The shear strains in the steel beam web of model T indicate the highest value, which is about 0.014, because of the lack of steel doubler plate. In comparison with the models F-B-S and S-T, use of TP would lead to about 2.8 times decrease in steel beam web shear strain in this model. The effects of eliminating the steel doubler plate in models with TP are depicted in Fig. 22(d). This figure illustrates that removing doubler plate in models with TP has no impressive impact on the performance of the model.

For models with the stronger beam, the inner concrete panel shear strains are shown in Fig. 22(a). The shear strains of the inner concrete panel in model T(s) indicate an increase at 1.35% storey drift and reach the peak value of about 0.025 at 4% storey drift. This increase in model F-B-S(s) happened at 1.28% storey drift and reached the peak value of about 0.041 at 4% storey drift. However, in Fig. 22(b) and with a comparison between models F-B-S and T, it could be understood that using TP instead of steel doubler plate causes about 40% decrease in shear strains of the outer concrete panel because of TP distributes stresses in a more area of the outer concrete panel.

The shear strains in the steel beam web of models with stiffer beam are presented in Fig. 22(c). As it could be realized, the shear strain values of the model F-B-S are greater from other models in accordance to the concrete failure in panel zone and the lack of proper transfer of loads to the concrete. The behavior of the tube plate is almost the same as the previous category.

In Figs. 22(a) and (b), due to the increase in the capacity of beams and column an increase in the shear strain of concrete panel in all of the models could be observed.

The shear performance of web of steel beam is almost the same as the second category. Fig. 22(d), exhibited the same shear performance of the tube plate with a little difference that it should be the result of increasing in the capacity of the beam.

5. Conclusions

In this paper, a new detail for circular reinforced concrete column steel beam (CRCS) connections using steel tube plate at the beam-column connection is proposed**.** Two interior connections were tested under quasi-static reversed cyclic loading. Furthermore; different interior beam-through type RCS connections are simulated using a nonlinear three-dimensional finite element method using ABAQUS software, which are verified with these experimental tests. Results demonstrated that:

- According to experimental results, the beam and longitudinal reinforcement of the column reached their yield capacity and at the panel zone of both specimens, beams have been yielded. In the specimen with SDP, level of strain in the panel zone is smaller than that in the specimen without SDP. According to the results the stiffness retaining to the capacity of specimens 1 and 2 are close to each other, and the SDP effect on the connection stiffness is less than 7 %.
- According to experimental and numerical results, the SDP increased the yielding capacity of the connection but it's effect on the maximum capacity of the connection, in different models are up to 8% (maximum different in the result is 8%).
- Due to the use of TP in the connection, the confinement of inner concrete panel would increase and the shear deformations of the panel zone compared to the common models have significantly decreased.
- Specimens under cyclic loading experienced no intense damage at the panel zone even that this part is the first place that show the nonlinear behavior. The beam-column connection of the specimens performed as a rigid connection according to the AISC 341-16. The CRCS system with tube plate demonstrated good ductility and good resistance to the shear forces and bending moments. This type of structural system has a good energy dissipation capacity.
- According to the finite element result, using the TP improves the performance of the panel zone by providing better confinement to the concrete at the panel zone. Moment-rotation curves indicated stable hysteresis behaviour without pinching. TP contributed to the increase in both rotational stiffness and moment-carrying capacity under cyclic loading conditions.
- Utilizing SDP has a slight effect on the lateral stiffness of the specimens, but it has a significant impact on the dissipated energy in which; specimen 1 saves 20% more energy dissipation in comparison with specimen 2 at the end. Both specimens tolerated almost the same maximum load. The results also showed that the SDP had a small effect on the shear strength, stiffness, and maximum capacity of the connection.
- Employing the tube plate at the panel zone is very suitable, and it could absorb and distribute stress in this region. Due to the good resistance against shear loads and moments, it could be used as an alternative for steel or concrete moment frames in high seismic risk zones.
- Application of TP, reduced the steel beam web participation in joint shear force and increased the TP and inner concrete panel participation. At 4% storey drift, fewer cracks are observed because the concrete panel was confined with TP. Using TP instead of steel doubler plate causes shear strains in the outer concrete panel, inner concrete panel and steel beam web in the panel zone to decrease.
- Experiments and modelling proved in models that failure occurs in the connection, addition of the SDP to the samples with TP increase the yielding and ultimate strength less than 10%. Also; the capacity, ductility and yielding strength models with TP are better than F-B-S models, and it seems that adding SDP is not necessary for samples with TP.

References

ABAQUS (2010), Abaqus analysis user's manual—version 6.10-1. Pawtucket, RI: Hibbit, Karlsson & Sorenson.

Alizadeh, S., Attari, N.K.A. and Kazemi, M.T. (2013), "The seismic performance of new detailing for RCS connections", *J. Construct. Steel Res.*, **91**, 76-88. https://doi.org/10.1016/j.jcsr.2013.08.010

Alizadeh, S., Attari, N.K.A. and Kazemi, M.T. (2015), "Experimental investigation of RCS connections performance using self-consolidated concrete", *J. Construc. Steel Res.*, **114**, 204-216. https://doi.org/10.1016/j.jcsr.2015.07.026

ANSI/AISC 341-16 (2016), Seismic Provisions for Structural Steel Buildings, American Institute of Steel Construction.

ASCE41-17 (2017), American Society of Civil Engineers, seismic evaluation and Upgrade of existing buildings, Reston, Virginia.

ASCE Task Committee on Design Criteria for Composite Structures in Steel and Concrete (1994), Guidelines for design of joints between steel beams and reinforced concrete columns, *J. Struct. Eng. ASCE*, **120**(8), 2330-2357.

ASTM A572/A572M-12 (2012), Standard Specification for High-Strength Low-Alloy Columbium-Vanadium Structural Steel.

ASTM A615/A615M-12 (2012), Standard Specification for Deformed and Plain Carbon-Steel Bars for Concrete Reinforcement.

Comité Euro-International du Béton (CEB-FIP Model Code 1990), International Recommendation for the Design and Construction of Concrete Structures. Thomas Telford, UK.

Cordova, P. and Deierlein, G.G. (2005), "Validation of the seismic performance of composite RCS framed: full-scale testing, analytical modeling, and seismic design", Report No. 155; Department of Civil and Environmental Engineering, Stanford University, CA, USA.

Ghods, S., Kheyroddin, A., Nazeryan, M., Mirtaheri, S.M. and Gholhaki, M. (2016), "Nonlinear behavior of connections in RCS frames with bracing and steel plate shear wall", *Steel Compos. Struct., Int. J.*, **22**(4), 915-935. http://dx.doi.org/10.12989/scs.2016.22.4.915

Kanno, R. (1993), "Strength, deformation, and seismic resistance of joints between steel beams and reinforced concrete columns", Ph.D. Dissertation; Cornell University, Ithaca, NY, USA.

Men, J., Guo, Z. and Shi, Q. (2015a), "Experimental research on seismic behavior of novel composite RCS joints", *Steel Compos. Struct., Int. J.*, **19**(1), 209-221.

http://dx.doi.org/10.12989/scs.2015.19.1.209
Men, J., Zhang, Y., Guo, Z. and Shi, Q. (2015b), "Experimental research on seismic behavior of composite RCS frame", *Steel Compos. Struct., Int. J.*, **18**(4), 971-983. http://dx.doi.org/10.12989/scs.2015.18.4.971

Nguyen, X.H., Nguyen, Q.H., Le, D.D. and Mirza, O. (2017), "Experimental study on seismic performance of new RCS connection", *Structures*, **9**(1), 53-62. https://doi.org/10.1016/j.istruc.2016.09.006

Nishiyama, I., Kuramoto, H. and Noguchi, H. (2004), "Guidelines: seismic design of composite reinforced concrete and steel buildings", *J. Struct. Eng. ASCE*, **130**(2), 336-342.

Parra-Montesinos, G. and Wight, J.K. (2001), "Modeling shear behavior of hybrid RCS beam-column connections", *J. Struct. Eng. ASCE*, **127**(1), 3-11. https://doi.org/10.1016/j.jcsr.2013.08.010

Sheikh, T.M., Deierlein, G.G., Yura, J.A. and Jirsa, J.O. (1989), "Beam–column moment connections for composite frames, part 1", *J. Struct. Eng. ASCE*, **115**(11), 2858-2876. https://doi.org/10.1061/(ASCE)0733-9445(1989)115:11(2858)

Thai, H.T., Uy, B. and Aslani, F. (2017), "Behaviour of bolted endplate composite joints to square and circular CFST columns", *J. Constr. Steel Res.*, **131**, 68-82. https://doi.org/10.1016/j.jcsr.2016.12.022

Zhang, X., Zhang, J., Gong, X. and Zhang, S. (2017), "Seismic performance of prefabricated high-strength concrete tube column–steel beam joints", *Adv. Struct. Eng.*, **21**(5), 658-674. https://doi.org/10.1177/1369433217726895

BU